MATERIALS PHYSICS AND MECHANICS RESEARCH ARTICLE

Submitted: June 12, 2025 **Revised: January 20, 2026** **Accepted: January 28, 2026**

Multiple surface crack interaction of non-coplanar cracks

O.M. Al-Moayed [1,2] ✉, A.E. Ismail [3], A.K. Kareem [4], S. Jamian [3]

[1] Department of Scientific Affairs, University of Anbar, Ramadi, Iraq

[2] Renewable Energy Research Centre, University of Anbar, Ramadi, Iraq

[3] Faculty of Mechanical and Manufacturing Engineering, University Tun Hussein Onn Malaysia, Batu Pahat, Malaysia

[4] Biomedical Engineering Department, College of Engineering and Technologies, Al-Mustaqbal University, Babil, Hillah, Iraq

✉ omar.m.f@uoanbar.edu.iq

ABSTRACT

Hollow cylinders represent one of the important elements in the industry. It is widely recognized that fracture characterizes the predominant mode of failure in cylindrical structures, which is precipitated by inherent imperfections or flaws. Over a period, these imperfections (cracks) may propagate and culminate in catastrophic failure, thereby presenting considerable hazards to both the surrounding ecosystem and human safety. Cracks can be single or multiple, and when they are in the multiple form, they can interact to increase pressures that are higher than what the material can withstand. Thus, this paper examines the influence of the interaction between double parallel non-coplanar cracks located on the external surface of a thick hollow cylinder subjected to remote tension and bending loading. Two sorts of separation distances were examined in this study, horizontal (s) and angular (α). The obtained stress intensity factor via finite element analysis was used to quantify the interaction factor along the crack front. The obtained results exhibited that both amplification and shielding interaction impacts could be observed along the crack front for a non-coplanar crack configuration. Additionally, both cracks exhibited the same interaction influence, but in opposite directions. The angular separation distance exhibited a significant influence on the interaction factor, this impact was strongly affected by the shape of the crack.

KEYWORDS

surface cracks • thick cylinder • semi-elliptical crack • crack interaction • non-coplanar cracks

Citation: Al-Moayed OM, Ismail AE, Kareem AK, Jamian S. Multiple surface crack interaction of non-coplanar cracks. *Materials Physics and Mechanics*. 2026;54(1): 57–72.
http://dx.doi.org/10.18149/MPM.5412026_7

Introduction

Hollow cylinders are fundamental components in engineering structures such as aerospace systems, pressure vessels, and pipelines. They are frequently subjected to cyclic loading, internal pressure, and harsh environmental conditions. The development of surface cracks in these structures, due to fatigue, stress corrosion, or manufacturing defects, poses a substantial risk to structural integrity [1]. While single cracks have been broadly studied, the presence of multiple interacting cracks can lead to accelerated crack growth, unexpected stress concentrations, and premature failure. Understanding these interactions is crucial for ensuring the safety and reliability of critical infrastructure. The interaction between multiple surface cracks in hollow cylinders remains a complex and insufficiently understood phenomenon. Closely spaced cracks can influence each other's growth through mechanisms demonstrated by either shielding or amplification [2].

This interaction complicates fracture predictions and challenges conventional damage tolerance assessments. Given the potential for catastrophic failures in industrial applications, a deeper investigation into crack interaction effects is essential for improving design standards and maintenance strategies. One of the important criterions in fracture mechanics is the stress intensity factors (SIFs), which can be used efficiently to characterize the crack interaction, particularly in the linear elastic fracture mechanics problems [3].

According to an analysis of cylinder failures that have occurred in service, most of them fall under the fracture sort, meaning that a flaw or crack grows and eventually causes the cylinder to fail [4]. Thus, surface cracks have been widely considered in the literature, either in plates or cylinders (solids and hollow). An efficient numerical method to compute SIFs and simulate coalescence and crack interaction is introduced by [5]. The study integrates principles of fracture mechanics to define fatigue failure to include modelling guidelines for practical implementation. The results revealed that, compared to fracture toughness-based criteria, through-thickness failure provides somewhat more conservative fatigue life predictions. Also, in [6], it was presented a modified strain-based J-integral method using 3D elastic-plastic finite element analysis (FEA). The modified method was utilized to assess circumferential cracks in pipelines subjected to internal pressure and large axial deformation. An analysis of the crack behavior was conducted in [7] by using SIF and J-integral assessment. The failure analysis was performed numerically for a semi-elliptical crack located on a total hip prosthesis. Also, the propagation of a short fatigue crack was predicted in [8] based on a non-local fracture criterion. The study considered non-monotonic crack expansion rate as well as estimating the existence of a single or multiple thresholds of SIF. Besides, in [9], it was experimentally and numerically examined the coalescence and growth of multiple interacting surface cracks. The study displayed that the behavior of crack coalescence was predictable; the study suggests that this method is scalable for multiple-crack structures, maintenance supporting, and safety assessment in engineering structures. In order to predict the crack behavior under dynamic loading [10] examined the stress intensity factors as well as the displacement fields in a rotating hollow cylinder containing an internal crack ring beneath axisymmetric torsion. In another study [11], the plastic stress intensity factor was validated as a more accurate predictor of fatigue life than traditional elastic SIFs. Hence, fatigue crack growth was investigated in a hollow cylinder with a semi-elliptical crack subjected to cyclic tension, torsion, and combined loading. The results indicated that crack growth was accelerated in combined loading compared to pure tension, consequently reducing the fatigue life. In addition, the relationship between SIF and crack velocity was examined numerically by [12]. The finite element methods (FEM) were employed to numerically examine cracks behavior in dual cantilever beam and single notch edge notched samples.

On the other hand, the behavior of cracks caused by explosive loading or blasting was experimentally investigated in [13,14]. A detailed analysis was introduced on the influence of the horizontal and vertical separation distances offsetting the cracks in terms of crack interaction. The stress concentration and distribution along the crack tips were considered. Likewise, the interaction influence between external and internal semi-elliptical cracks located in a pressurized cylinder was investigated via the hybrid boundary element method (HBEM) by [15]. The results showed that both cracks displayed SIFs less

than those of isolated (single) cracks. Also, stronger interaction effects were observed for shallow, long cracks. In addition, in [16], it was conducted FEA to evaluate mode I SIFs for single and multiple semi-elliptical cracks positioned in an internally pressurized hollow cylinder for high crack aspect ratios. Based on the results, an empirical formula has been presented to facilitate the prediction of fatigue life as well as integrity assessments in pressurized cylinders. Similarly, the interaction phenomenon in a pressurized cylinder containing two coplanar surface cracks was performed using FEA [17]. This study indicated that there is a direct proportion between the internal pressure and the crack interaction. A 3D FEA was conducted in [18,19] for a hollow cylinder containing an embedded elliptical crack with a semi-elliptical crack, where the Crack Tip Opening Displacement method (CTOD) was applied. The crack orientation, separation distances, and internal pressure levels were examined. The findings displayed that the most severe fracture response was attained under tension loading combined with a high rate of internal pressure. Furthermore, the interaction impact of two similar circumferential cracks on the limit load analysis was investigated in [20]. Therefore, FEA was performed for various crack geometries and interaction criteria. The study proposed new combination rules and indicated that existing codes are conservative, particularly for coplanar cracks, as later supported by [21].

Based on the surveyed literature, it can be concluded that surface crack interaction has been extensively examined. The diversity of these studies lies in one of the following: the cracked body, the crack (orientation, location, and geometry), the number of cracks, separation distances, and loading types. In addition, it has been proven that the SIF criterion is a suitable parameter that could be employed to quantify the interaction phenomenon. Furthermore, several methods can be used to determine the SIFs; however, FEA is more efficient for performing such analyses. Thus, this paper numerically investigates the impact of angular separation distance α (overlapping) on crack interaction. The crack interaction of double parallel non-coplanar cracks is quantified by calculating the interaction factor based on the SIFs. Moreover, different crack geometries and crack separation (horizontal and angular) distances were considered to investigate the influence of the separation distances and crack geometries on crack interaction. The distribution of the normalized SIFs is introduced first, followed by the interaction factor, and finally, the relationship between the angular separation distance and the SIFs is addressed.

Layout of the problem

This study numerically examines a hollow cylinder with double neighboring non-coplanar surface cracks located on the external surface, subjected to separate tension and bending loading as shown in Fig. 1. As described in Fig. 1, this study utilized a straight hollow homogeneous cylinder, with material properties and dimensions explained in Tables 1 and 2, respectively.

It should be noted that both cracks are located on the external surface of the cylinder, and are similar in shape and size, the shape is controlled by a/c, while the depth is controlled by a/t, where a and c represent the depth and length of the crack, respectively. Furthermore, a/c varies from 0.4 to 1.2 to include a variety of slender and transverse crack shapes.

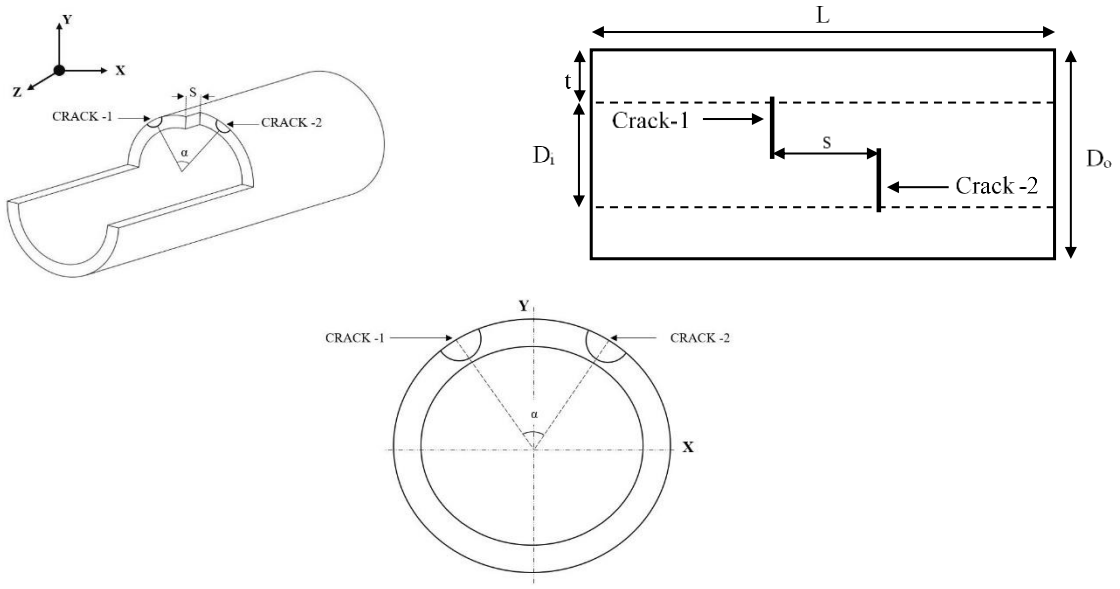

Fig. 1. Problem layout

Table 1. Material properties

Property	**Value**
Young's modulus, GPa	200
Poisson's ratio	0.3
Tensile yield strength, MPa	250
Tensile ultimate strength, MPa	460

Table 2. Cylinder dimensions

Parameter	**Value**
Internal diameter D_i, mm	200
Outer diameter D_o, mm	250
Wall-thickness t, mm	25
Length L, mm	750
t/R_i	0.25

Table 3. Crack geometry

a/c	***a/t***	***a*, mm**	***c*, mm**
0.4	0.2	5	12.5
	0.5	12.5	31.25
	0.8	20	50
0.6	0.2	5	8.3333
	0.5	12.5	20.833
	0.8	20	33.333
0.8	0.2	5	6.25
	0.5	12.5	15.625
	0.8	20	25
1.0	0.2	5	5
	0.5	12.5	12.5
	0.8	20	20
1.2	0.2	5	4.1666
	0.5	12.5	10.416
	0.8	20	16.666

Similarly, *a/t* changes between 0.2, 0.5, and 0.8 to ensure testing shallow and deep cracks throughout the thickness. The examined crack geometries are listed in Table 3.

On the other hand, referring to Fig. 1, the cracks are separated by two separation distances, horizontal (*s*) and angular (α) with respect to the Y-axis. Both horizontal and angular separation distances are recorded in Table 4, where (*s*) is described by the normalized form *s/L*. It should be noted that the *s/L* range was considered as recommended by [22]. It has been reported that 13 mm is the maximum distance at which crack interaction can be detected; otherwise, cracks are considered separate. This means that when the distance between cracks is more than 13 mm, each crack should be considered a single or isolated crack. Therefore, the examined *s/L* reflects the suggested distance and beyond. The purpose of examining beyond stated limits is to verify separation rules.

Table 4. Horizontal and angular separation distances

s/L	α, °
0.004	10, 20, 30
0.008	10, 20, 30
0.016	10, 20, 30
0.032	10, 20, 30

Methods

Due to the intricacy of the geometry, finite element methods (FEM) are an effective tool in tackling multiple crack interaction issues [23]. Thus, in this work, the double cracks problem has been modeled and analyzed using Ansys, the finite element (FE) software. Additionally, the stress intensity factor (SIF) is utilized to define the crack interaction phenomenon, where the calculated SIFs are then normalized for each loading type according to the following [24]:

$$F_t = \frac{K_{cal,t}}{\sigma_t \sqrt{\pi a/Q}}, \quad (1)$$

where F_t is the normalized SIFs under remote tension loading, $K_{cal,\,t}$ is the calculated SIFs under tension (extracted from Ansys), σ_t is the axial stress, where $\sigma_t = P/\pi\,(R^2_o - R^2_i)$, P is the remote applied force, and R_o and R_i represent the outer and inner radius of the cylinder, individually. Besides, a is the crack depth, and Q is the shape factor defined by [25]:

$$Q = 1 + 1.464(a/c)^{1.65} \text{ for a/c} \leqslant 1, \quad (2)$$

$$Q = 1 + 1.464(c/a)^{1.65} \text{ for a/c} > 1. \quad (3)$$

On the other hand, for bending loading, the SIFs are normalized according to the following equation [26], where F_{Ben} is the standardized SIFs underneath remote bending, $K_{cal,\,b}$ is the calculated SIFs under bending (which are extracted from Ansys), σ_b is the maximum bending stress:

$$F_{Ben} = \frac{K_{cal,b}}{\sigma_b \sqrt{\pi a/Q}}. \quad (4)$$

After obtaining the normalized SIFs for each type of loading, as previously discussed, the interaction factor has to be identified. In order to calculate the interaction factor Ψ, which is defined as the ratio of the nondimensional SIFs for the case of two cracks to that of a single crack, the following equation is utilized [27]:

$$\Psi = \frac{F_{two\ cracks}}{F_{single\ crack}}. \quad (5)$$

It should be remarked that $F_{two\ cracks}$ and $F_{single\ crack}$ denote standardized SIFs for the case of two and single cracks, respectively. This procedure applies to all examined configurations and loading types. Furthermore, it should be noted that Ψ describes the crack interaction impact, where (Ψ = 1) indicates that there is no crack interaction, while (Ψ < 1) shows that shielding impact, and (Ψ > 1) illustrates the amplification influence between the cracks.

Results

This section introduces the obtained results in this study, where the orientation of the SIFs along the crack front is discussed first, then the interaction factor, and finally, the influence of the inclination angle on the crack interaction is investigated. It ought to be noted that the exploited model for this research was the same as that which has been used by [28].

Distribution of SIFs

The distribution of the normalized SIFs along the crack front is presented in this section, where the normalized SIFs for different crack geometrical parameters are introduced as a function of the normalized crack front position, $2\theta/\pi$. Furthermore, any point on the crack front is described by using θ, where $-90 \leqslant \theta \leqslant 90$, as shown in Fig. 2. Thus, $2\theta/\pi = 1$ at point A, 0 at point B, and -1 at point C.

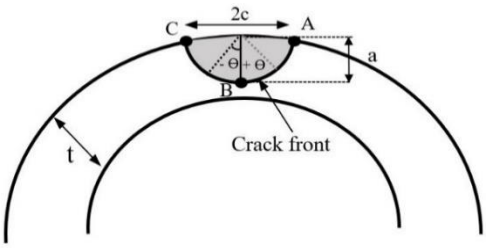

Fig. 2. Crack geometry with points on the crack front

Due to the similar trend revealed by the SIFs with respect to α of the two cracks under each tension and bending loading, the normalized SIFs of one crack for $a/c = 0.4$ and 1.2 are presented in this section for $\alpha = 10°$ only. On the other hand, the remaining values are discussed in terms of the impact of α with respect to a/c. It should be noted that the normalized SIF for the case of a single crack is presented in figures epitomized by F_SINGLE, while SIFs of two cracks are categorized based on the horizontal separation distance, F2 – s/L (0.004, 0.008, 0.016, 0.032).

Figure 3 shows the trend of the normalized SIFs for external noncoplanar parallel cracks under remote tension loading, F_t, for inclination angle α=10°, when $a/c = 0.4$ for $a/t = 0.2$, 0.5, and 0.8. Due to cracks overlapping, the interaction between the cracks affected the overall curve shape of the F2 for the double cracks compared to F_SINGLE. In the case of completely parallel cracks [28], the trend of the normalized SIFs for double parallel cracks followed an exactly similar curve to that of F_SINGLE for all the examined s/L, except it was less in value due to the shielding phenomenon. However, in the presence of overlapping between cracks, F2 for all examined s/L ratios exhibited amplification and shielding effects simultaneously.

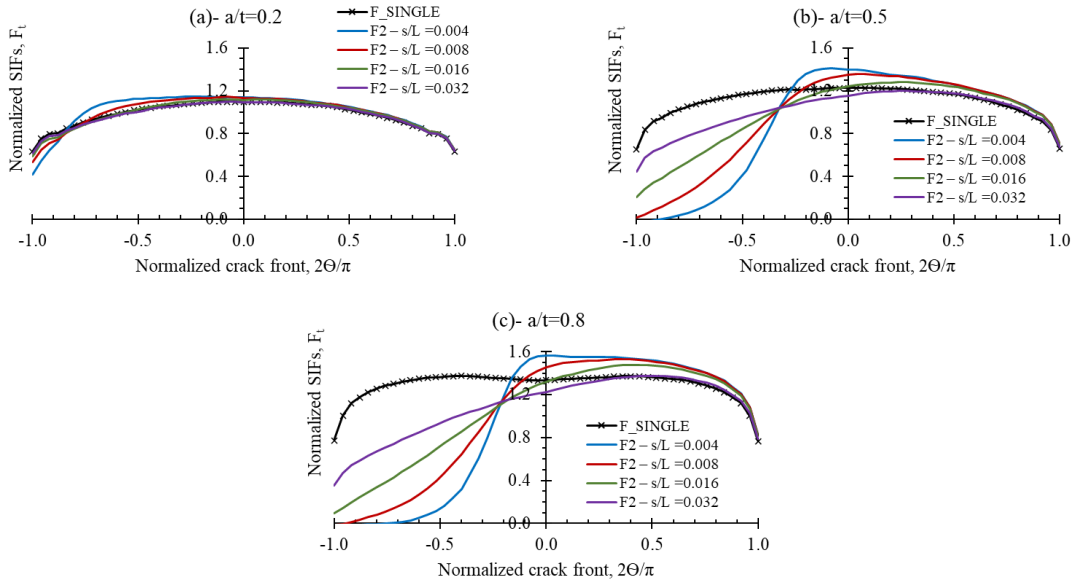

Fig. 3. SIFs under tension for a/c = 0.4, α = 10°

Additionally, Fig. 3 revealed that for a specific crack shape ratio, a/c, the relative depth of the crack, a/t, has a strong influence on F_t. Moreover, for a/t = 0.2, this impact was found to be tiny for all inspected s/L, while for $a/t \geqslant 0.5$, the impact was more pronounced for all observed s/L values. On the other hand, the shielding effect occurs within the zone of cracks overlap, while the amplification appears at the point of overlapping, radiates outward, and subsequently decays.

Furthermore, from Fig. 3, it can be inferred that s/L displayed insignificant influence on the crack interaction for $a/t < 0.5$, while for $a/t \geqslant 0.5$, the effect was more distinct. The maximum crack interaction influence was attained for F2 – s/L= 0.004, which is the smallest horizontal separation distance between the cracks, while the minimum was observed for F2 – s/L = 0.032. Despite s/L = 0.032 being greater than the limits introduced in [22], it is obvious that F2 – s/L = 0.032 did not approach F_SINGLE, due to the presence of a crack interaction, and the two cracks can not be considered isolated. Thus, relying on [22] for structural integrity assessment could lead to underestimation or conservative results, as confirmed by [29]. Moreover, it has been stated that the usage of combination rules presents too much conservatism in the assessment, especially for interacting cracks.

Similarly, Fig. 4 illustrates the normalized SIFs' orientation for non-coplanar cracks exposed to remote tension loading for a/c = 1.2 when the inclination angle, α = 10°. The increase in the crack aspect ratio displayed that a/t behaved in the same manner that was remarked for small a/c, except that the interacting cracks were isolated when reaching the maximum separation distance, s. This might be interpreted as a high a/c; the depth of the crack is greater than the length of the crack, accordingly, the length of the crack has a significant impact on the SIFs.

Alternatively, for shallow cracks, a/t = 0.2, the crack interaction was found to be insensitive to the change in horizontal separation distance, while for a/t = 0.5, the crack interaction was demonstrated by the amplification effect only. As well, for deep cracks, a/t = 0.8, the interaction among the cracks demonstrated by both shielding and magnification, which is the same behaviour that has been noticed for a/c = 0.4.

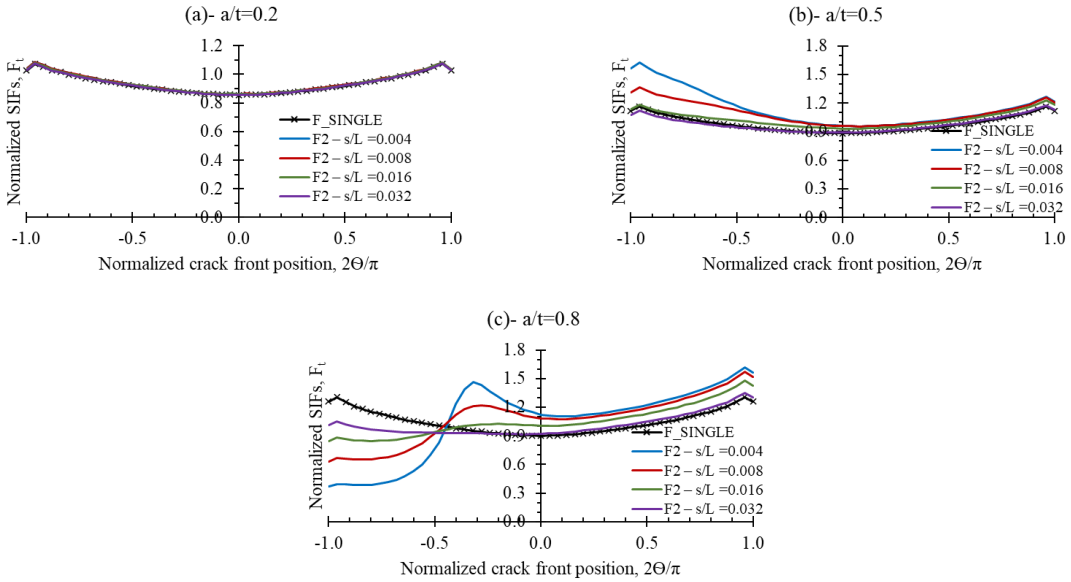

Fig. 4. SIFs under tension for a/c = 1.2, α = 10°

Figures 5 and 6 display the diffusion of the standardized SIFs for the non-coplanar parallel cracks under remote bending loading, F_{Ben}, for the overlapping ratio defined by α = 10°, when a/c = 0.4 and 1.2 for a/t = 0.2, 0.5, and 0.8. Apparently, the distribution of F_{Ben} for all evaluated s/L exhibited a similar trend to that found under tension loading, except that the bending SIFs are slightly less. Additionally, F_{Ben} tendency shown bared that a/t has a notable influence on F_{Ben}, however, for a/t = 0.2, this effect was found to be negligible for all tested s/L ratios, whereas for a/t = 0.5 and 0.8, the impact was more evident for all s/L. Also, it can be inferred that for low and high crack aspect ratios, shallow cracks ($a/t \leqslant 0.4$), were found to be unresponsive to the change in s/L, the impact is extra remarkable for higher values. Nevertheless, the interacting cracks were isolated when s/L = 0.032 for a high aspect ratio, while for a low aspect ratio, the influence of each crack on the other still exists.

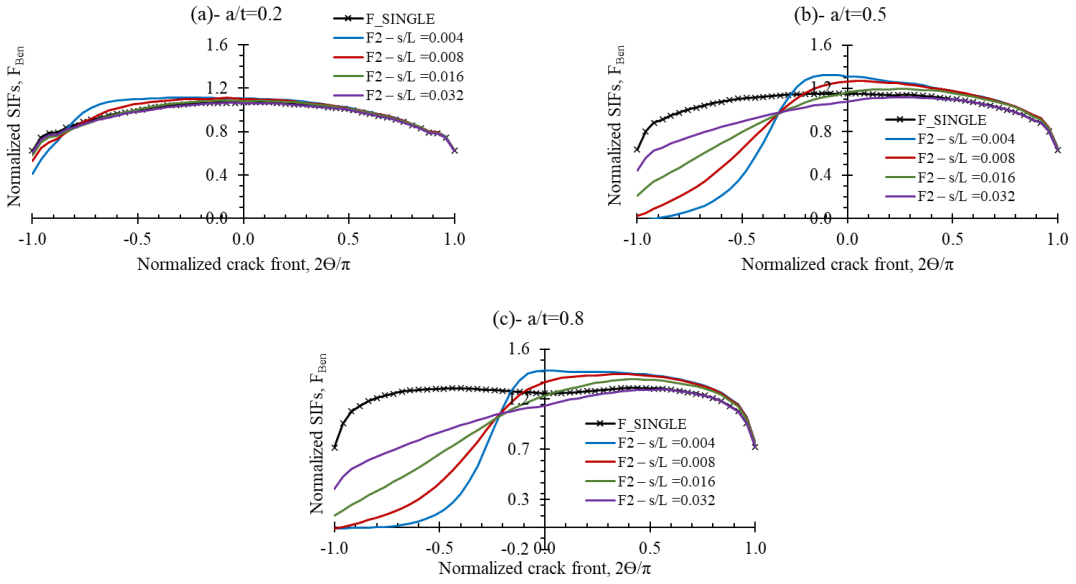

Fig. 5. SIFs under bending for a/c = 0.4, α = 10°

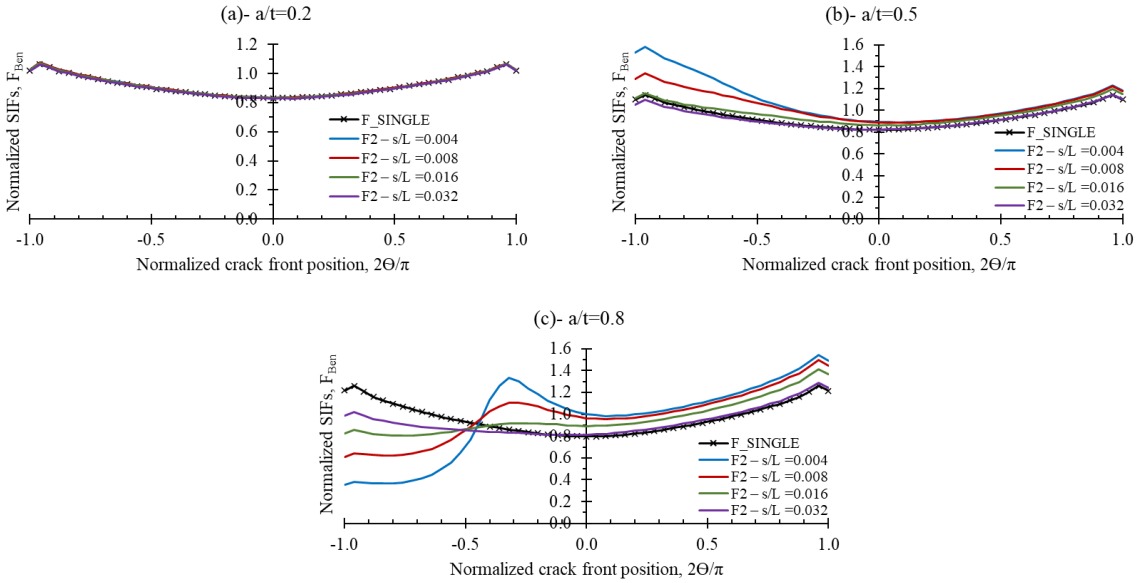

Fig. 6. SIFs under bending for *a/c*=1.2, α = 10°

Interaction factor

This section introduces the interaction factor Ψ, which is calculated by Eq. (5), for external non-coplanar parallel cracks subjected to remote tension loading for the examined crack geometry presented in the previous section, α = 10°, for *a/c* = 0.4 and 1.2. Moreover, the remaining examined configuration will be discussed in the next section in terms of the effect of the inclination angle. It should be noted that *Ψ* is presented for three points on the crack front A, B, and C, as shown in Fig. 2, A and C are the edge points, and C is the point that lies inside the overlapping zone, while B is the deepest point on the crack front. Furthermore, the influence of crack interaction on SIFs could be demonstrated by three classes. Firstly, enhancement (amplification), which is attained when nondimensional SIFs of two cracks are higher than those of a single crack. The second category is the shielding impact, which is the opposite of amplification; standardized SIFs of a single crack are greater than those of two cracks. Third class is the no interaction situation, when no significant difference in the SIFs of single and double cracks; thus, each crack is treated as an isolated crack. It is worth declaring that this study assumed that, for (Ψ = 1 ± 0.05), there was no interaction, which is the same tolerance ratio considered by [30]. Table 5 elucidates the interaction factor Ψ for external parallel non-coplanar cracks exposed to remote tension when α = 10°, *a/c* = 0.4 for different crack depths.

Table 5. Ψ for noncoplanar parallel cracks under tension when α = 10°, *a/c* = 0.4

a/t	Point	*s/L* = 0.004	*s/L* = 0.008	*s/L* = 0.016	*s/L* = 0.032
0.2	**A**	1.024	1.017	1.015	1.007
	B	1.040	1.037	1.019	0.998
	C	0.657	0.839	0.930	0.969
0.5	**A**	1.060	1.061	1.053	1.019
	B	1.142	1.101	1.014	0.943
	C	-0.036	0.024	0.318	0.683
0.8	**A**	1.081	1.077	1.065	1.026
	B	1.174	1.090	0.991	0.916
	C	-0.015	-0.023	0.123	0.461

Furthermore, it can be observed that *s/L* exhibited a substantial influence on Ψ. This impact was recognized by magnification and shielding, where the maximum interaction influence was observed for small *s/L*, representing the closest distance between the two cracks. This impact gradually diminished as the two cracks became isolated. In fact, at the maximum examined separation distance *s/L* = 0.032, the cracks with *a/t* = 0.2 have been isolated, and there is no discernible influence between the cracks at A, B, and C. On the other hand, cracks with *a/t* ⩾ 0.5, have no interaction influence at point A, which is the farthest point from the overlapping region, while at points B, and C, the F_t did not approach F_SINGLE, therefore, Ψ value was less than 1.0, which means crack interaction is still affecting. It is worth noting that the negative values of Ψ, which have been seen at point C, for *s/L* = 0.004, denote a change in the crack opening direction, which was changed due to the interaction effect from opening mode to closing mode.

In addition, for the maximum horizontal separation distance *s/L* = 0.032, at point A (the distant point from the region that overlaps), no crack interaction effect is recognized for all examined *a/t*. Equally, an approximately similar trend was recognized at point B (the deepest point at the crack front). However, at point C, the impact of crack interaction still exists when *a/t* = 0.8, where the SIFs value reduction equals 53.9 %.

Table 6 illustrates the quantified interaction factor for non-coplanar interacting cracks subjected to tension loading when $\alpha = 10°$, *a/c* = 1.2. Unlike for shallow cracks (*a/c* = 0.4), Ψ is shown to be insensitive to the change in *s/L* for *a/t* = 0.2, where all Ψ values approach 1 at all crack front points (A, B, and C) for all examined *s/L*, which indicates no interaction. On the other hand, for *a/t* = 0.5, a slight amplification impact has been noticed at points A and B, while at point C, Ψ increased by about 39.6 % due to interaction when *s/L* = 0.004.

Table 6. Ψ for non-coplanar parallel cracks under tension when $\alpha = 10°$, *a/c* = 1.2

a/t	Point	*s/L* = 0.004	*s/L* = 0.008	*s/L* = 0.016	*s/L* = 0.032
0.2	A	1.007	1.007	1.007	1.001
	B	1.005	1.006	1.006	0.999
	C	1.011	1.012	1.008	1.001
0.5	A	1.085	1.078	1.055	1.011
	B	1.087	1.085	1.055	1.007
	C	1.396	1.175	1.012	0.958
0.8	A	1.241	1.205	1.135	1.035
	B	1.249	1.205	1.117	1.022
	C	0.293	0.503	0.673	0.804

Table 7. Interaction factor Ψ, under tension loading for *a/c* = 0.4 and 1.2

a/t	Points	*s/L* = 0.004		*s/L* = 0.032	
		a/c = 0.4	*a/c* = 1.2	*a/c* = 0.4	*a/c* = 1.2
0.2	A	1.024	1.007	1.007	1.001
	B	1.040	1.005	0.998	0.999
	C	0.657	1.011	0.969	1.001
0.5	A	1.060	1.085	1.019	1.011
	B	1.142	1.087	0.943	1.007
	C	-0.036	1.396	0.683	0.958
0.8	A	1.081	1.241	1.026	1.035
	B	1.174	1.249	0.916	1.022
	C	-0.015	0.293	0.461	0.804

Meanwhile, for a/t = 0.8, magnification impact was recognized at each A and B, and this influence gradually decreased until reaching the maximum s/L. Yet, at C, a reduction in the SIFs resulted due to the crack interaction in terms of shielding impact, the SIFs decreased by 70.7 % when s/L = 0.004. It should be noted that when s/L = 0.032 exceeds the (13 mm) recommended by [22], Ψ did not approach 1, which means that both cracks still affect each other. This result aligns with the observed impact for a/c = 0.4 under tension loading as mentioned earlier.

It should be noted that by examining points A, B, and C in Tables 5 and 6, under tension loading, the increment in a/c displayed different impacts on Ψ, as shown in Table 7. The documented behavior for s/L = 0.004, points A and B presented similar performance in terms of amplification, shielding, and no interaction, except Ψ for a/c = 1.2, slightly higher. However, at point C, for s/L = 0.004, a shielding influence was recognized for a/c = 0.4, while no interaction was found at the same point for a/c = 1.2. In addition, for a/t = 0.5, at point C, 39.6 % enhancement resulted due to the change in crack shape, a/c = 1.2, while a complete reduction was found for a/c = 0.4. It is possible to clarify this discrepancy in terms of the shape of the crack, which strongly influences the interaction phenomenon; deep sharp cracks (a/c = 1.2) have more opportunity to show amplification effect than shielding, unlike wide shallow cracks (transverse cracks). On the other hand, despite s/L = 0.032 exceeding the limits suggested in [22], crack interaction is still remarkable at point C, especially for $a/t \geqslant 0.5$. Again, the results indicated that the present crack interaction alignment rules might produce underestimation in the stresses or conservative results.

Table 8. Ψ for noncoplanar parallel cracks under bending when α = 10°, a/c = 0.4

a/t	Point	s/L = 0.004	s/L = 0.008	s/L = 0.016	s/L = 0.032
0.2	**A**	1.010	1.004	1.001	0.994
	B	1.037	1.033	1.015	0.994
	C	0.662	0.844	0.937	0.975
0.5	**A**	1.042	1.043	1.036	1.002
	B	1.139	1.097	1.009	0.937
	C	-0.030	0.037	0.334	0.695
0.8	**A**	1.046	1.042	1.031	0.992
	B	1.172	1.085	0.983	0.908
	C	-0.011	-0.011	0.144	0.484

Table 9. Ψ for noncoplanar parallel cracks under bending when α = 10°, a/c = 1.2

a/t	Point	s/L = 0.004	s/L = 0.008	s/L = 0.016	s/L = 0.032
0.2	**A**	1.002	1.002	1.002	0.996
	B	1.001	1.003	1.003	0.995
	C	1.008	1.009	1.005	0.998
0.5	**A**	1.074	1.068	1.045	1.002
	B	1.087	1.084	1.053	1.003
	C	1.392	1.172	1.012	0.960
0.8	**A**	1.226	1.190	1.122	1.024
	B	1.259	1.213	1.121	1.020
	C	0.292	0.503	0.676	0.809

Tables 8 and 9 describe Ψ for non-coplanar parallel interacting cracks subjected to bending loading when $\alpha = 10°$ for $a/c = 0.4$ and 1.2. In general, Ψ behavior was similar to that obtained under tension loading for similar a/c, where s/L exhibited a significant effect on Ψ; as soon as s/L declined, the impact of crack interaction decreased. In addition, cracks with $a/t = 0.2$ were isolated for $s/L = 0.032$ at each of A, B, and C, but for cracks with $a/t \geq 0.5$, the interaction effect was still pronounced, especially at point C, the nearest point to the second crack.

Influence of angular separation distance

In order to visualize the relationship between the inclination angle and the normalized SIFs in terms of crack interaction, it is necessary to present the SIFs as a function of the inclination angle (or could be used as the overlapping angle). Based on the results presented in the previous section, it was found that the maximum interaction influence was always attained when $s/L = 0.004$ and $a/t = 0.8$. Where $s/L = 0.004$ demonstrates the smallest separation distance between the cracks, while $a/t = 0.8$ represents the deepest relative crack depth ratio. Therefore, the separation distance $s/L = 0.004$ and $a/t = 0.8$ have been selected to present the effect of inclination angle on the distribution of the normalized SIFs since both ratios produced the maximum interaction influence.

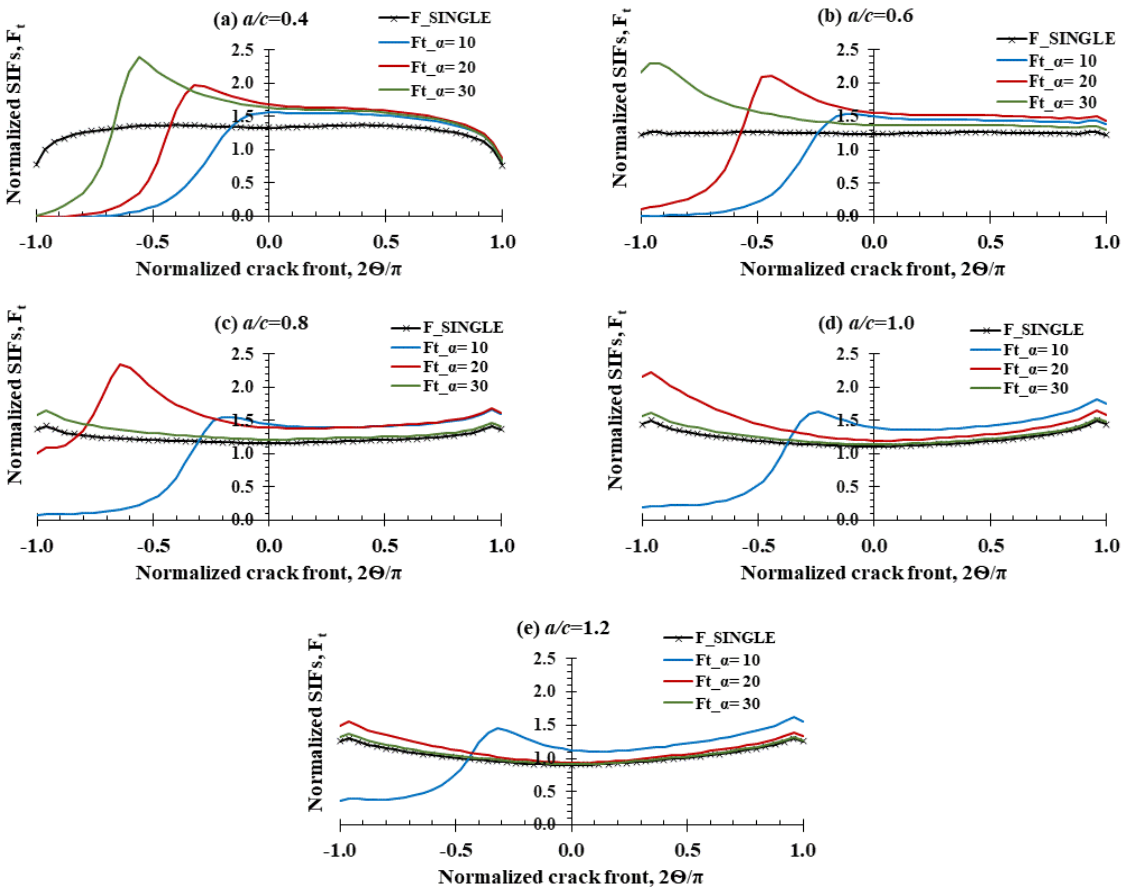

Fig. 7. Relationship between (α) and (*a/c*) for $a/t = 0.8$, and $s/L = 0.004$ under tension loading

Figure 7 displays the impact of different inclination angles on the distribution of the normalized SIFs as a function of the crack aspect ratio, *a/c*, under remote tension loading for a non-coplanar parallel cracks configuration when *s/L* = 0.004 and *a/t* = 0.8. Furthermore, to comprise a wide diversity of crack shapes, the crack aspect ratio is considered to be varied from 0.4 to 1.2, which has been presented in Fig. 7(a–e), respectively. Also, the considered inclination angles are α = 10, 20, and 30°.

Obviously, the inclination angle α has a significant influence on crack interaction behavior, and this effect strongly depends on the examined *a/c*, which has produced different impacts. The increase in the *a/c* ratio is accompanied by the decrease in F_t, which indicates that sharp cracks are riskier or more serious than transverse cracks, where for the same α value, the peak F_t is attained when *a/c* = 0.4, while the minimum is when *a/c* = 1.2.

On the other hand, α produced unique behaviors, depending on the examined *a/c*. Moreover, for α = 10°, the F_t distribution followed an approximately similar trend along the crack front with respect to the change in *a/c*, where the amplification effect was noticed in the region from $2\theta/\pi$ = -0.2 to 1.0 on the crack front, and the shielding effect was recognized from $2\theta/\pi$ = -0.2 to -1, this effect applied to all examined *a/c* ratios, where with the increase of *a/c*, the area that experiences the amplification impact increases also.

Also, for α = 20°, the F_t was distributed in two different styles, for *a/c* < 1.0, F_t exhibited both amplification and shielding effects along the crack front, whilst for *a/c* ⩾ 1.0, a severe amplification effect was noticed in the overlapping zone, and a minor amplification impact was observed far away from the overlapping zone. It should be noted that during the change in *a/c* from 0.8 to 1.0 for α = 20°, the F_t behavior switched from the shielding and amplification mixed behavior to the pure amplification impact.

Similarly, for α = 30°, it has been found that for this inclination angle, the influence on the F_t distribution was more pronounced for *a/c* ⩽ 0.8, where it presented both interaction influences amplification and shielding. It should be noted that throughout the change in *a/c* from 0.4 to 0.6 for α = 30°, the F_t behavior exhibited pure amplification impact instead of the combination of shielding and amplification impacts. Moreover, for *a/c* ⩾ 1.0, the inclination angle α = 30° has no significant influence on the distribution of F_t along the crack front.

In the same way, Fig. 8 displays the relationship between α and the normalized SIFs under bending F_B. It is obvious that the impact of α on F_B was found to be similar to that obtained under tension loading, except that F_B was less than F_t. This influence is understandable since SIF for the case of a single crack under tension loading is higher than that under bending loading. However, it was found that the positions where the maximum SIFs are attained along the crack front under each tension and bending are similar, as indicated in Table 10.

Table 10. Maximum normalized SIFs under different types of loading

a/c	α = 10°				α = 20°				α = 30°			
	$2\theta/\pi$	F_t	$2\theta/\pi$	F_B	$2\theta/\pi$	F_t	$2\theta/\pi$	F_B	$2\theta/\pi$	F_t	$2\theta/\pi$	F_B
0.4	0	1.56	0	1.40	-0.32	1.97	-0.32	1.79	-0.56	2.39	-0.56	2.19
0.6	-0.08	1.54	-0.08	1.38	-0.44	2.11	-0.44	1.93	-0.92	2.29	-0.92	2.16
0.8	0.96	1.66	0.96	1.57	-0.64	2.34	-0.64	2.18	-0.96	1.64	-0.96	1.55
1.0	0.96	1.82	0.96	1.72	-0.96	2.22	-0.96	2.12	-0.96	1.61	-0.96	1.53
1.2	0.96	1.61	0.96	1.54	-0.96	1.55	-0.96	1.48	-0.96	1.36	-0.96	1.29

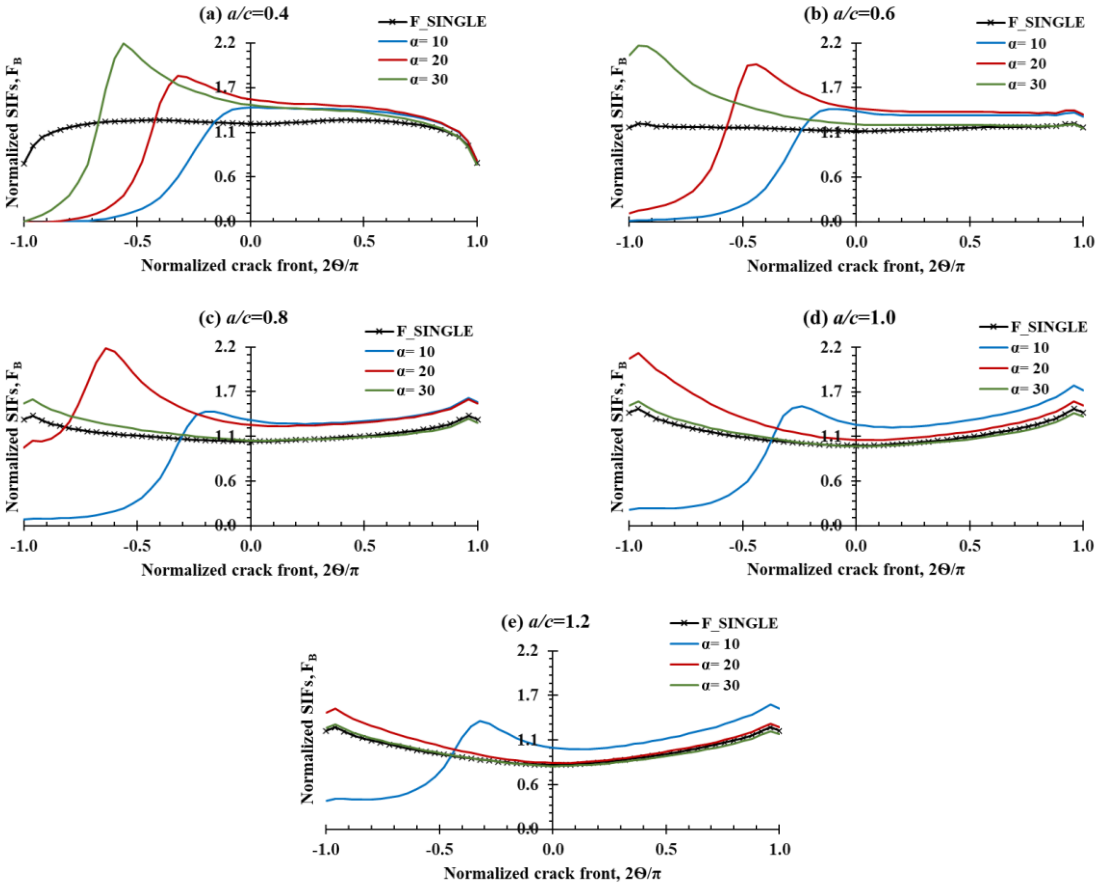

Fig. 8. Relationship between (α) and (a/c) for a/t = 0.8, and s/L = 0.004 under bending loading

The position on the crack front is defined by the normalized form ($2\Theta/\pi$), where Θ is the parametric angle of the crack, $2\Theta/\pi$ = 0 (B, at the deepest point), 1 (A, farthest point with respect to the overlapping zone), and -1 (C, the point within the overlapping zone) Fig. 2. From Table 10, it can be inferred that the maximum F_t and F_B were attained at the same position on the crack front for all examined a/c. Furthermore, for $a/c \leqslant 0.6$, the increase in α was accompanied by an increment in F_t and F_B, while for $0.6 < a/c \leqslant 1.0$, when α advances, F_t and F_B rise until $\alpha = 30°$, where both F_t and F_B exhibited a drop in value. Finally, for $a/c > 1.0$, the increase in the overlap region between the cracks produced a decrease in F_t and F_B. This indicates that the interaction phenomenon reduces as the cracks turn into a transverse shape with respect to the increment in the overlapping angle.

Conclusion

The impact of crack orientation on surface crack interaction has been investigated numerically via finite element analyses. A thick hollow cylinder was considered with double parallel non-coplanar cracks with different crack geometries subjected to tension and bending loading. Based on the results, the interaction influence for the non-coplanar cracks showed amplification and shielding impacts simultaneously along the crack front. The shielding effect is recognized on one side of the crack front (in the overlapping region), while the other side of the crack front shows the amplification effect. This inconsistency in the interaction influence is triggered by the non-coplanar orientation.

Moreover, in the region of overlap, the shielding effect occurs due to the partial parallel orientation, thus the shielding impact appears. But, on the other side of the crack front or the region out of the overlapping zone, the amplification effect occurs. This indicates that for such kinds of crack configurations, the riskiest region is the zone that lies outside the parallel case, or simply, there is no crack in front of this region. This is because the crack will propagate from this region and lead to cylinder failure. It is evident that the presence of the second crack in a completely (or partially) parallel orientation will provide more resistance to the cylinder, where a mutual closing effect is offered by the two cracks towards each other. It should be noted that the inclination angle (or the angular distance), along with a change in *a/c*, provided a unique influence on the SIFs allocation. Furthermore, both α and *a/c* have a significant impact on the crack interaction, since both can convert Ψ from pure shielding to amplification, which may lead to crack extension.

CRediT authorship contribution statement

Omar Mohammed Al-Moayed: writing – original draft, conceptualization, data curation; **Al Emran Ismail**: writing – review & editing, conceptualization, supervision; **Ali Kamil Kareem**: writing – original draft, investigation, data curation; **Saifulnizan Jamian**: writing – review & editing, supervision, investigation.

Conflict of interest

The authors declare that they have no conflict of interest.

References

1. Yang Y, Lam CC, Kou KP. Fatigue life analysis of internal circumferential crack of tubular structures. *International Journal of Damage Mechanics*. 2015;24(5): 711–727.
2. Wang H, Liu Z, Xu D, Zeng Q, Zhuang Z. Extended finite element method analysis for shielding and amplification effect of a main crack interacted with a group of nearby parallel microcracks. *International Journal of Damage Mechanics*. 2016;25(1): 4–25.
3. Anderson TL. *Fracture mechanics: fundamentals and applications*. 4th ed. Boca Raton: CRC press; 2017.
4. Marshall P. *The residual structural properties of cast iron pipes: structural and design criteria for linings for water mains*. UKWIR; 2001.
5. Mishael J, Morato PG, Rigo P. Numerical fatigue modeling and simulation of interacting surface cracks in offshore wind structural connection. *Marine Structures*. 2023;92: 103472.
6. Zhao D, Gao W, Zhao K, Zheng H, Chen J, Yu J, Zheng Z. A strain-based J-integral formulation for an internal circumferential surface crack of pipeline under inner pressure and large axial deformation. *International Journal of Pressure Vessels and Piping*. 2024;212: 105316.
7. Zahaf S, Dahmane M, Belaziz A, Bouri I, Afane N. Failure analysis of semi-elliptical crack behavior in the cement mantle of a total hip prosthesis. *Materials Physics and Mechanics*. 2022;48(2): 242–271.
8. Nosikov AI, Semenov AS, Melnikov BE, Rayimberdiyev TP. Prediction of short fatigue crack propagation on the base of non-local fracture criterion," *Materials Physics and Mechanics*. 2017;31(1–2): 44–47.
9. Kikuchi M. Study on multiple surface crack growth and coalescence behaviors. *AIMS Mater Sci*. 2016;3(4): 1623–1631.
10. Zhuravlova Z, Istenes I, Peck D, Protserov Y, Vaysfeld N. Hidden ring crack in a rotating hollow cylinder under torsion. *Int J Eng Sci*. 2024;194: 103976.
11. Shlyannikov V, Yarullin R, Ishtyryakov I. Surface crack growth in cylindrical hollow specimen subject to tension and torsion. *Fracture and Structural Integrity*. 2015;9(33): 335-344.
12. Kazarinov NA, Petrov YV, Bratov VA, Slesarenko VY. Numerical investigation of stress intensity factor — crack velocity relation for a dynamically propagating crack. *Materials Physics and Mechanics*. 2016;29(1): 39–42.

13. Peng L, Yue Z, Wang X, Zhou J. Experimental study on the interaction mechanism of two dynamic cracks under blasting loading. *International Journal of Rock Mechanics and Mining Sciences*. 2024;184: 105956.
14. Peng L, Yue Z, Wang X, Zhou J. Experimental study on interaction characteristics of explosive cracks under confining pressure and its comparison with free boundary results. *Journal of Materials Research and Technology*. 2024;33: 4637–4653.
15. Guozhong C, Zhimin F, Xianfeng J, Gan L. Analyses on interaction of internal and external surface cracks in a pressurized cylinder by hybrid boundary element method. *International Journal of Pressure Vessels and Piping*. 2004;81(5): 443–449.
16. Kirkhope KJ, Bell R, Kirkhope J. Stress intensity factors for single and multiple semi-elliptical surface cracks in pressurized thick-walled cylinders. *International Journal of Pressure Vessels and Piping*. 1991;47(2): 247–257.
17. Kim D. S, Lo KH. Crack Interaction Criteria in Pressure Vessels and Pipe. *Journal of Offshore Mechanics and Arctic Engineering*. 1995;117(4): 260–264.
18. Zhang YM, Ariffin MZ, Xiao ZM, Zhang WG, Huang ZH. Nonlinear elastic--plastic stress investigation for two interacting 3-D cracks in offshore pipelines. *Fatigue Fract Eng Mater Struct*. 2015;38(5): 540–550.
19. Zhang Y, Fan M, Xiao Z. Nonlinear elastic-plastic stress investigations on two interacting 3-D cracks in offshore pipelines subjected to different loadings. *AIMS Mater Sci*. 2016;3(4): 1321–1339.
20. Kamaya M. A combination rule for circumferential surface cracks on pipe under tension based on limit load analysis. *J Press Vessel Technol*. 2011;133(2): 021205.
21. Coêlho GC, Silva AA, Santos MA, Lima AGB, Santos NC. Stress Intensity Factor of Semielliptical Surface Crack in Internally Pressurized Hollow Cylinder—A Comparison between BS 7910 and API 579/ASME FFS-1 Solutions. *Materials*. 2019;12(7): 1042.
22. American Petroleum Institute (API) and the American Society of Mechanical Engineers (ASME). *Fitness-For-Service API 579-1/ASME FFS-1*. Washinghton, DC: ASME; 2016.
23. Alshoaibi AM, Fageehi YA. Advances in Finite Element Modeling of Fatigue Crack Propagation. *Applied Sciences*. 2024;14(20): 9297.
24. Mohammed O, Kareem AK, Jamian S, Nemah MN. Distribution of mode I stress intensity factors for single circumferential semi-elliptical crack in thick cylinder. *International Journal of Integrated Engineering*. 2019;11(7): 102–111.
25. Newman JC, Raju IS. An empirical stress-intensity factor equation for the surface crack. *Eng Fract Mech*. 1981;15(1): 185–192.
26. Al-moayed OM, Kareem AK, Ismail AE, Jamian S, Nemah MN. Influence Coefficients for a single superficial cracked thick cylinder under torsion and bending moments. *International Journal of Integrated Engineering*. 2020;12(4): 132–144.
27. Jamian SFS, Abed TH, Aldulaymi OH. Interaction Assessment of Stress Intensity Factors of Surface Cracks on Thick Cylinders under Tension Force and Bending Moment. *Journal of Advanced Research in Applied Mechanics*. 2024;118(1): 131–143.
28. Al-Moayed OM, Ismail AE, Kareem AK, Jamian S, de C. Coêlho G. Interaction of double parallel cracks located on a hollow cylinder. *Latin American Journal of Solids and Structures*. 2023;20(10): e514.
29. Coêlho G, Silva A, Santos M. Elastic surface crack interaction and its engineering critical assessment within the framework of fitness-for-service standards. *Frattura Ed Integrità Strutturale*. 2022;16(60): 134–145.
30. Anis SF, Koyama M, Hamada S, Noguchi H. Simplified stress field determination for an inclined crack and interaction between two cracks under tension. *Theoretical and Applied Fracture Mechanics*. 2020;107: 102561.